Metal–Organic Frameworks

International Edition: DOI: 10.1002/anie.201503588
German Edition: DOI: 10.1002/ange.201503588

Organization and Energy Transfer of Fused Aromatic Hydrocarbon Guests within Anion-Confining Nanochannel MOFs**

*Tae Hwan Noh, Haeri Lee, Jaeseong Jang, and Ok-Sang Jung**

Abstract: *The self-assembly of Zn^{II} ions with 1,3,5-tris(isonicotinoyloxyethyl)cyanurate produces new topological $(4^2{\cdot}12^4)_3(4^3)_4$ 2D metal–organic frameworks (MOFs) with anion-confining cages. The eclipsed assembly of each 2D MOF by π–π stacking of cyanurate moieties (3.352(5) Å) forms 3D MOFs consisting of nanochannels (10.5 Å). Two of the three anions are confined in each peanut-type cage, resulting in hydrophobicity of the nanochannels. The hydrophobic nanochannel effectively adsorbs a wide range of fused aromatic hydrocarbons (FAHs) as monomers or dimers, rendering it potentially highly useful as an energy-transfer material.*

Nanochannel materials have been employed for the past two decades as host networks for useful guest molecules with such host–guest systems having been found to show intriguing electrochemical, optical, and magnetic properties.[1] Thus, formation and functionalization of metal–organic frameworks (MOFs) with task-specific channels present interesting possibilities for tuning of guest conformations, guest preorganization, and unusual transition states.[2] Meanwhile, fused aromatic hydrocarbons (FAHs), recognized as harmful pollutants,[3] are known to have interesting photophysical properties. Anthracene and pyrene, for example, recently have been found in the ultraviolet light emitted by the red rectangle nebula.[4] Inclusion of two or more guest FAHs in a channel affords a particular type of recognition or energy-transfer (ET) system depending on the distance and relative orientation of the donor–acceptor pair.[5] The unique fluorescence properties of FAHs within hosts undoubtedly are mediated by π–π stacking interactions, hydrogen bonds, and van der Waals interactions.[6] To date, cyclodextrins[7] and rectangular cyclophanes[8] have been employed as hosts for incorporation of isolated FAH species from bulk FAHs. However, studies focusing systematically on the details of the organization of FAHs in MOFs for recognition and ET remains unexplored, although some examples of γ-cyclodextrin,[9] DNA,[10] and coordination cages[11] as host molecules for the formation of excimeric FAH species have been reported. Herein, we report the fabrication of hydrophobic nanochannel MOFs $[Zn_3L_4(CH_3CN)_6](X)_6$ (L = 1,3,5-tris(isonicotinoyloxyethyl)-cyanurate; $X^- = BF_4^-$ and ClO_4^-) by assembly of octahedrally coordinated Zn^{II} centers with C_3-symmetric tridentate N-donor ligands. In these MOFs, FAHs have been directly included, organized, and preliminary Förster resonance energy transfer (FRET) of FAHs within the nanochannels was reported. To our knowledge, this is the first example of the inclusion of FAHs and subsequent FRET within a MOF.

Self-assembly of ZnX_2 with C_3-symmetric ligand L produces single crystals composed of $[Zn_3L_4(CH_3CN)_6](X)_6{\cdot}5\,CH_2Cl_2{\cdot}3\,H_2O$ suitable for single-crystal X-ray diffraction, as depicted in Scheme 1. The crystalline product could be successfully obtained irrespective of the concentrations and mole ratios, indicating that the product is the most thermodynamically favorable species. The crystals were insoluble in water and other common organic solvents including acetone, benzene, chloroform, tetrahydrofuran, and toluene. The crystals slowly lost their crystallinity in air owing to the evaporation of the solvated molecules on the surface, but their basic structures were very stable under anaerobic conditions.

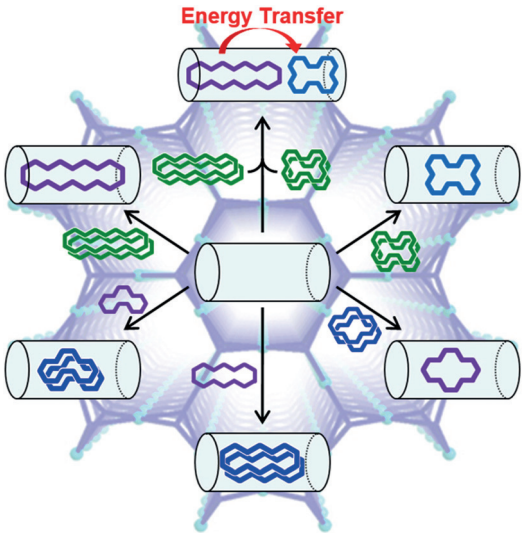

Scheme 1. The inclusion of FAHs in $[Zn_3L_4(CH_3CN)_6](X)_6$ nanochannels ($X^- = BF_4^-$ and ClO_4^-).

The structure of $[Zn_3L_4(CH_3CN)_6](BF_4)_6{\cdot}5\,CH_2Cl_2{\cdot}3\,H_2O$ is very similar to that of $[Zn_3L_4(CH_3CN)_6](ClO_4)_6{\cdot}5\,CH_2Cl_2{\cdot}3\,H_2O$, except for the counterions (Figure 1). From a topological point of view (see Figure S1 in the Supporting Information), L acts as a 3-connected node and the Zn^{II} ion acts as a 4-connected node to construct a 2D

[*] Dr. T. H. Noh, H. Lee, J. Jang, Prof. Dr. O.-S. Jung
Department of Chemistry, Pusan National University
Jangjeon-dong, Geumjeong-gu, Pusan 609-735 (Korea)
E-mail: oksjung@pusan.ac.kr

[**] This work was supported by the National Research Foundation of Korea (NRF) grant funded by the Korean Government (MEST; 2013R1A2A2A07067841). MOF = metal–organic framework.

Supporting information for this article is available on the WWW under http://dx.doi.org/10.1002/anie.201503588.

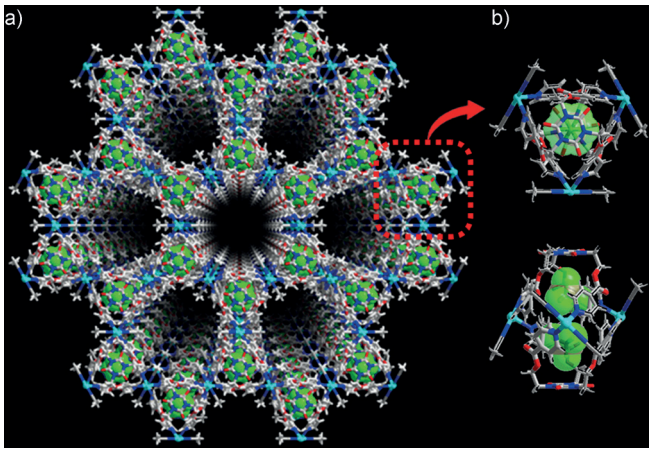

Figure 1. Crystal structure of $[Zn_3L_4(CH_3CN)_6](BF_4)_6{\cdot}5CH_2Cl_2{\cdot}3H_2O$: a) packing structure of 2D networks showing 1D nanochannels and b) top and side views of one $[Zn_3L_2(CH_3CN)_6]^{6+}$ unit. The included BF_4^- ions are represented as space-filling models.

coordination polymer which has a new binodal 3,4-connected net topology with the point symbol $(4^2{\cdot}12^4)_3(4^3)_4$.[12] Specifically, the two tridentate L bridge three Zn^{II} ions in a helical conformation, thereby forming a truncated trigonal bipyramidal $[Zn_3L_2]$ peanut-type cage moiety that is occupied by two BF_4^- ions.[13] The distance between the two cyanuric planes is 13.216(3) Å, and the Zn···Zn separation is 10.6887(2) Å. Thus, the cage has an elliptical cavity of dimensions $4.1\times4.1\times10.0$ Å^3. It is noteworthy that two of the three BF_4^- ions are nestled within the cavity (Figure 1b) and that the other is positioned in the void space of the unit cell. Considering the ligand conformation, the cage moiety has right-handed (*P*) and left-handed (*M*) helicity[14] in alternating fashion in the solid state (Figure S2), resulting in a hexagonal cavity with a diagonal Zn···Zn distance of 21.3774(4) Å. As depicted in Figure S3, the void diameter of the hexagonal cavity is 10.5 Å. The most interesting structural feature is that the 2D layers are tightly packed, resulting in the formation of a 3D framework consisting of nanochannels along the *c* axis (Figure 1),[15] while the interlayer π···π distance between the cyanuric planes is 3.352(5) Å (Figure S4). Notably, the channels are occupied by dichloromethane, water, and one-third of the anions. The free volume of the channels is, based on PLATON calculations,[16] 3553.5 Å^3/6562.7 Å^3, which is 54.1 % of the crystal volume.

The coordination network construction is outlined in Figure S5. The C_3-symmetric tridentate N-donor ligand is a key triangular building block for self-assembly of the 2D kagome-type network by coordination to Zn^{II} ions. The combination of the geometry of Zn^{II} centers with L, having an appropriate length and conformation, is an important factor for formation of the new topological 2D network. The frameworks have sustainable nanosized channels that are occupied by solvate dichloromethane and water molecules and partially by anions. In this case, anions serve as structure-directing templates for building the cages that encapsulate them. In effect, confinement of two of the three anions in the cages makes the nanochannels relatively hydrophobic. The other anions in these nanochannels are highly disordered, meaning that the nature of their interactions with the channels remains unclear. The collaboration between the π–π interactions and the unique anion-confining cages might be an important factor for the construction of the desired hydrophobic channel materials.

FAHs, such as anthracene (ANT), pyrene (PYR), perylene (PER), phenanthrene (PHE), and naphthacene (NAP), were used as dyes for incorporation into the nanochannels described herein. Single crystals of Zn-MOF were immersed in an *n*-hexane solution of each FAH and allowed to stand for three days without heating or stirring, which resulted in formation of the inclusion composites FAH⊂Zn-MOF (see the Supporting Information for experimental details). Solid-state photoluminescence (PL) measurements were carried out in order to investigate the FAHs entrapped within the Zn-MOF, the results of which are in Table 1. As depicted in Figure S6, L and Zn-MOF, upon excitation at $\lambda = 365$ nm, displayed weak emission bands at around 465 and 463 nm, respectively, indicating that the emission originated from a ligand-centered transition.

Table 1: Fluorescence emission maxima (λ_{em}) and quantum efficiencies (Φ)[a] for free FAHs and FAH⊂$[Zn_3L_4(CH_3CN)_6](BF_4)_6$ composites.

	FAH: solution[b] λ_{em} [nm] (Φ)	FAH: solid[b] λ_{em} [nm]	Composite: solid λ_{em} [nm] (Φ)
Anthracene (ANT)	monomer	monomer	dimer
	405 (0.36)	424	480 (0.10)
Phenanthrene (PHE)	monomer	monomer	dimer
	367 (0.34)	411	479 (0.07)
Pyrene (PYR)	monomer	dimer[18]	monomer
	376 (0.43)	463	407 (0.50)
Naphthacene (NAP)	monomer	dimer[17b]	monomer
	479 (0.33)	566	450 (0.04)
Perylene (PER)	monomer	dimer[17a]	monomer
	443 (0.94)	568	478 (0.02)

[a] The quantum efficiency for the free FAHs was measured in $CHCl_3$ solution using Firpic ($\Phi = 0.42$) as the standard. [b] Measured for the free FAH (i.e. not in the inclusion complex) in solution (methanol/dimethyl sulfoxide, v/v = 4:1) and in the solid state.

For PER and NAP, the free FAHs (before inclusion) showed excimeric emission with $\lambda_{max} = 568$ and 566 nm ($\lambda_{ex} = 365$ nm) in the solid state, respectively. The structures of PER and NAP are known to be dimeric in the solid state.[17] In contrast, the included species exhibited emission maxima at $\lambda_{max} = 478$ and 450 nm, respectively, indicating that the FAH species are organized as monomers within the channels to form PER⊂Zn-MOF and NAP⊂Zn-MOF. The PL spectra of PER⊂Zn-MOF and NAP⊂Zn-MOF in solution in methanol/dimethyl sulfoxide (v/v = 4:1) are very similar to the spectra of the free FAH molecules, indicating complete dissociation of the FAH molecules from the MOF nanochannels (Figure 2b and Figure S7). Similarly, in the case of PYR, the free PYR showed excimeric emission with $\lambda_{max} = 463$ nm ($\lambda_{ex} = 365$ nm) in the solid state, whereas PYR⊂Zn-MOF exhibited relatively sharp monomeric PYR emission with $\lambda_{max} = 407$ nm (Figure 2a). The structure of the PYR crystal is known to be composed of partially overlapping dimeric units.[18] In case of

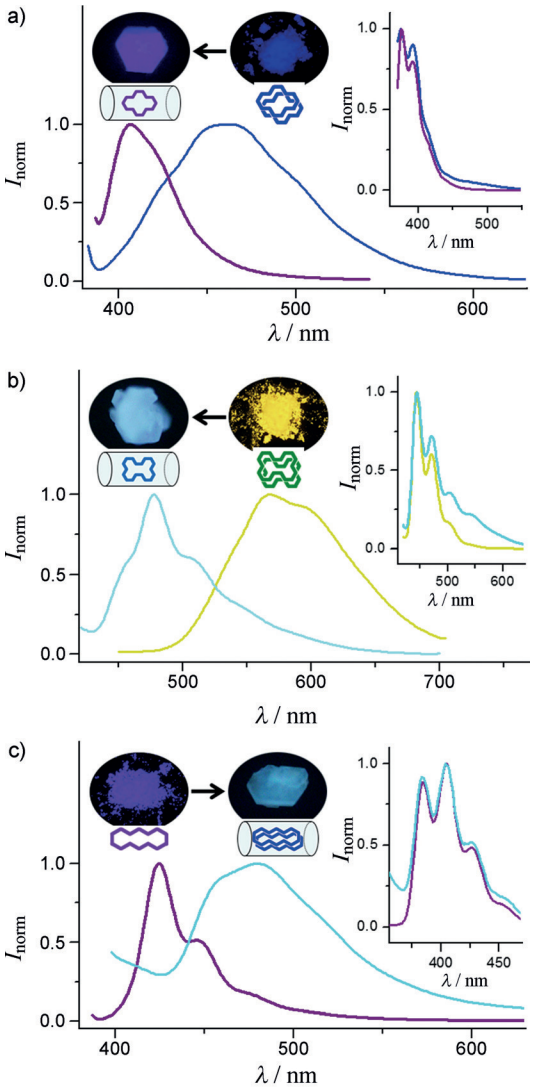

Figure 2. Solid-state PL spectra ($\lambda_{ex} = 365$ nm), fluorescence microscopy images, and schematic structural representation: a) PYR (blue) and PYR⊂Zn-MOF (purple); b) PER (yellow) and PER⊂Zn-MOF (cyan); c) ANT (purple) and ANT⊂Zn-MOF (cyan). Inset: PL spectra ($\lambda_{ex} = 365$ nm) in solution in methanol/dimethyl sulfoxide (v/v = 4:1) of the free FAHs and their corresponding included complexes.

several studies on pyrene inclusion within zeolites,[19] particularly faujasites which have supercages with a formal diameter of circa 13 Å, the organization of pyrene molecules within the zeolite was dependent on the concentration of the loaded pyrene solution. In the present work, on the other hand, single PYR molecules could not move past each other because the nanochannels were too narrow. Full inclusion could not be achieved even after a prolonged immersion process, presumably because of the presence of one of the three counterions and partial solvate molecules inside the channels.[20]

Interestingly, NAP and PER simultaneously enter into the nanochannels at similar rates, thereby providing a randomly ordered homogeneous distribution, denoted NAP·PER⊂Zn-MOF (see the Supporting Information for experimental details). As depicted in Figure 3b, the emission spectrum of NAP·PER⊂Zn-MOF upon excitation at $\lambda = 335$ nm, where the absorption of NAP is strong and that of PER is relatively weak, was dominated by a band at $\lambda = 472$ nm corresponding to the included PER, along with a shoulder band at $\lambda =$

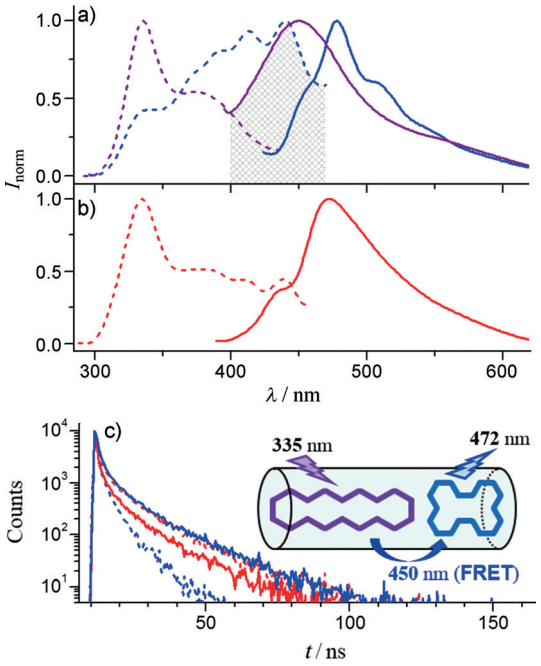

Figure 3. Solid-state excitation (dashed lines) and emission (solid lines) spectra of a) NAP⊂Zn-MOF (purple), PER⊂Zn-MOF (blue), and b) NAP·PER⊂Zn-MOF (red). c) Fluorescence lifetime decays following excitation at $\lambda = 375$ nm of NAP⊂Zn-MOF (monitored at $\lambda = 450$ nm; red dotted line), PER⊂Zn-MOF (monitored at 478 nm; blue dotted line), and NAP·PER⊂Zn-MOF (monitored at 450 (red) and 472 nm (blue); solid lines). Inset: schematic representation of FRET between included NAP and PER. Gray shaded section in (a): spectral overlap of the included NAP emission and PER excitation.

438 nm corresponding to the included NAP. This indicates that the emission corresponding to NAP was considerably quenched, whereas that corresponding to PER was significantly enhanced. As a result of the sufficient spectral overlap between NAP emission (as the donor) and PER absorption (as the acceptor), NAP·PER⊂Zn-MOF can participate in the FRET process. The same local fluorescence emission maxima at different excitation wavelengths (Figure S8) confirm that phenomenon. There was a small shift of the PER emission maxima, from $\lambda = 478$ nm for PER⊂Zn-MOF to 472 nm for NAP·PER⊂Zn-MOF, which occurred as a result of the decrease in self-absorption and re-emission of PER molecules within the nanochannels because of the decreased amount of PER. In time-resolved fluorescence experiments, the fluorescence lifetimes (τ) of the three composites were measured in order to better understand the photophysical properties; the corresponding fluorescence decay curves are depicted in Figure 3c. The fluorescence decays of NAP⊂Zn-MOF, PER⊂Zn-MOF, and NAP·PER⊂Zn-MOF in the solid-state were all fitted to biexponential curves. The fluorescence mean lifetime (τ_m)[21] of each NAP⊂Zn-MOF and PER⊂Zn-MOF excited at $\lambda = 375$ nm is 0.77 ns and 1.04 ns, respectively

(Table S1). The decay of NAP in NAP·PER⊂Zn-MOF, measured at 450 nm, had a shorter fluorescence mean lifetime of 0.75 ns, indicating that the energy transfer is from excited NAP to PER chromophores. Moreover, the decay of PER in NAP·PER⊂Zn-MOF (1.61 ns) was much longer than in PER⊂Zn-MOF, which might be ascribable to a large reorientation of PER fluorophores and a restriction of the rotational degrees of freedom owing to the stronger hydrophobic interactions between the NAP and PER chromophores in the nanochannels.[22] A follow-up detailed investigation of the mechanism and photophysical properties is currently underway. To our knowledge, this system is the first demonstrable example of the facile inclusion and energy transfer of FAH molecules within nanochannels of MOFs. Other mixed sorbate composites, NAP·PHE⊂Zn-MOF, PER·PHE⊂Zn-MOF, and PER·PYR⊂Zn-MOF, did not show the FRET phenomena, which might be ascribed to the insufficient spectral overlap between the emission spectrum of one FAH⊂Zn-MOF and the excitation spectrum of another FAH⊂Zn-MOF (Figure S9).

The free ANT and PHE molecules, as depicted in Figure 2c and Figure S6, respectively, showed strong emission in the solid state centered at $\lambda = 424$ and 411 nm, respectively, whereas the included complexes generated broad emission bands at $\lambda = 480$ and 479 nm, respectively. In light of the fact that ANT and PHE have been known to exist as monomers in the solid state and in dilute *n*-hexane solution,[23] the significant bathochromic shift was attributed to the occurrence of a dimeric π···π stacking orientation (known as *H*-type stacking[24]) of ANT and PHE within the nanochannels. These results suggest that the hydrophobic nanochannels accommodate the reorganization of FAH molecules resulting in the formation of dimeric FAHs within the channels to form $(ANT)_2$⊂Zn-MOF and $(PHE)_2$⊂Zn-MOF, respectively. The PL spectrum of $(ANT)_2$⊂Zn-MOF in solution in methanol/dimethyl sulfoxide (v/v = 4:1) was the same as that of the free ANT solution, indicative of dissociation of the FAH guest from the host nanochannels (Figure 2c).

At this stage, the exact mechanism for the formation of FAHs⊂Zn-MOF remains unclear, though most likely it arises from a combination of π···π and van der Waals interactions between FAH molecules themselves, and between FAH and the Zn-MOF skeletal structure inside the anion-confining nanochannels. Tight host–guest contact seems very important as the nanochannel is relatively hydrophobic. In order to clarify the factors influencing guest inclusion, a number of control experiments were carried out. The difference between employing $X^- = BF_4^-$ or ClO_4^- as counterion was found to be negligible (see Figure S10). The inclusion capacities of the FAHs were determined to be in the order PYR > ANT > NAP ≈ PER ≈ PHE. The solvent effects for inclusion were in the order *n*-hexane > benzene > diethyl ether > dioxane/dichloromethane (v/v = 4:1), which is inversely proportional to the polarity.

In conclusion, self-assembly of Zn^{II} ions with a C_3-symmetric tridentate ligand gives rise to the formation of new topological 2D networks with anion-confining cages. The 2D networks were assembled by π···π interactions to form unique 3D MOFs consisting of hydrophobic nanochannels, which serve as hosts for FAH recognition, inclusion, and organization. These phenomena are strongly dependent on the nature of the FAH and are mediated by π–π stacking interactions between FAHs and the channel properties of the MOFs. For NAP·PER⊂Zn-MOF, an efficient FRET process from the NAP to the PER was detected, as promoted by a large degree of spectral overlap between NAP emission and PER absorption. In combination, these results indicate that the energy transfer in these FAHs⊂MOF materials is achieved by π-electronic donor–acceptor interactions. Additional and more systematic studies on, for example, the synthesis of related ligands, are in progress. Further experiments, moreover, should provide more detailed information on energy transfer, adsorption–desorption properties, stable guest storage, and intra-channel reactivity.

Experimental Section

Synthetic, spectroscopic, and crystallographic data for $[Zn_3L_4(CH_3CN)_6](X)_6 \cdot 5\,CH_2Cl_2 \cdot 3\,H_2O$ ($X^- = BF_4^-$ and ClO_4^-), details of the inclusion of the FAHs, and all CIF files are included in the Supporting Information. CCDC 1060420 and 1060421 contain the supplementary crystallographic data for this paper. These data are provided free of charge by The Cambridge Crystallographic Data Centre.

Keywords: energy transfer · FRET · metal–organic frameworks · polyaromatic hydrocarbons · zinc

How to cite: *Angew. Chem. Int. Ed.* **2015**, *54*, 9284–9288
Angew. Chem. **2015**, *127*, 9416–9420

[1] a) Y. Wang, H. Li, Y. Feng, H. Zhang, G. Calzaferri, T. Ren, *Angew. Chem. Int. Ed.* **2010**, *49*, 1434–1438; *Angew. Chem.* **2010**, *122*, 1476–1480; b) N. S. Kehr, A. Schäfer, B. J. Ravo, L. De Cola, *Nanoscale* **2010**, *2*, 601–605; c) D. Brühwiler, G. Calzaferri, T. Torres, J. H. Ramm, N. Gartmann, L.-Q. Dieu, I. López-Duarte, M. V. Martínez-Díaz, *J. Mater. Chem.* **2009**, *19*, 8040–8067; d) J.-P. Zhang, Y.-B. Zhang, J.-B. Lin, X.-M. Chen, *Chem. Rev.* **2012**, *112*, 1001–1033; e) G. Calzaferri, S. Huber, H. Maas, C. Minkowski, *Angew. Chem. Int. Ed.* **2003**, *42*, 3732–3758; *Angew. Chem.* **2003**, *115*, 3860–3888; f) T. H. Noh, J. Jang, W. Hong, H. Lee, O.-S. Jung, *Chem. Commun.* **2014**, *50*, 7451–7454; g) M. Park, H. Kim, H. Lee, T. H. Noh, O.-S. Jung, *Cryst. Growth Des.* **2014**, *14*, 4461–4467.

[2] a) M. Ogawa, T. Ishii, N. Miyamoto, K. Kuroda, *Adv. Mater.* **2001**, *13*, 1107–1109; b) D. Yan, J. Lu, J. Ma, S. Qin, M. Wei, D. G. Evans, X. Duan, *Angew. Chem. Int. Ed.* **2011**, *50*, 7037–7040; *Angew. Chem.* **2011**, *123*, 7175–7178; c) N. Yanai, T. Uemura, M. Inoue, R. Matsuda, T. Fukushima, M. Tsujimoto, S. Isoda, S. Kitagawa, *J. Am. Chem. Soc.* **2012**, *134*, 4501–4504; d) T. Uemura, N. Uchida, A. Asano, A. Saeki, S. Seki, M. Tsujimoto, S. Isoda, S. Kitagawa, *J. Am. Chem. Soc.* **2012**, *134*, 8360–8363.

[3] a) A. Luch, *The Carcinogenic Effects of Polycyclic Aromatic Hydrocarbons*, Imperial College Press, London, **2005**; b) C.-E. Boström, P. Gerde, A. Hanberg, B. Jernström, C. Johansson, T. Kyrklund, A. Rannug, M. Tornqvist, K. Victorin, R. Westerholm, *Environ. Health Perspect.* **2002**, *110*, 451–488; c) D. Werner, C. P. Higgins, R. G. Luthy, *Water Res.* **2005**, *39*, 2105–2113.

[4] a) U. P. Vijh, A. N. Witt, K. D. Gordon, *Astrophys. J.* **2005**, *619*, 368–378; b) U. P. Vijh, A. N. Witt, K. D. Gordon, *Astrophys. J.* **2004**, *606*, L65–L68.

[5] a) T. Förster, *Ann. Phys.* **1948**, *437*, 55 – 75; b) T. Förster, *Discuss. Faraday Soc.* **1959**, *27*, 7 – 17; c) D. L. Dexter, *J. Chem. Phys.* **1953**, *21*, 836 – 850; d) K. B. Eisenthal, S. Siegal, *J. Chem. Phys.* **1964**, *41*, 652 – 655.
[6] a) Y. Tanaka, K. M.-C. Wong, V. W.-W. Yam, *Chem. Eur. J.* **2013**, *19*, 390 – 399; b) D. M. Sena, Jr., H. O. Pastore, F. B. T. Pessine, *Phys. Chem. Chem. Phys.* **2009**, *11*, 7219 – 7224; c) H. Kashida, H. Asanuma, M. Komiyama, *Chem. Commun.* **2006**, 2768 – 2770.
[7] a) L. A. Blyshak, K. Y. Dodson, G. Patonay, I. M. Warner, *Anal. Chem.* **1989**, *61*, 955 – 960; b) R. M. Mohseni, R. J. Hurtubise, *J. Chromatogr. A* **1990**, *499*, 395 – 410; c) H. Lamparczyk, P. Zarzycki, R. J. Ochocka, D. Sybilska, *Chromatographia* **1990**, *30*, 91 – 94; d) M. T. Butterfield, R. A. Agbaria, I. M. Warner, *Anal. Chem.* **1996**, *68*, 1187 – 1190; e) G. Shixiang, W. Liansheng, H. Qingguo, H. Sukui, *Chemosphere* **1998**, *37*, 1299 – 1305.
[8] a) J. C. Barnes, M. Juricek, N. L. Strutt, M. Frasconi, S. Sampath, M. A. Giesener, P. L. McGrier, C. J. Bruns, C. L. Stern, A. A. Sarjeant, J. F. Stoddart, *J. Am. Chem. Soc.* **2013**, *135*, 183 – 192; b) R. Lin, J. H. K. Yip, K. Zhang, L. L. Koh, K.-Y. Wong, K. P. Ho, *J. Am. Chem. Soc.* **2004**, *126*, 15852 – 15869; c) C. Peinador, E. Pía, V. Blanco, M. D. García, J. M. Quintela, *Org. Lett.* **2010**, *12*, 1380 – 1383.
[9] a) A. P. de Silva, N. Gunaratne, T. Gunnlaugsson, A. J. M. Huxley, C. P. McCoy, J. T. Rademacher, T. E. Rice, *Chem. Rev.* **1997**, *97*, 1515 – 1566; b) M. Toda, N. Ogawa, H. Itoh, F. Hamada, *Anal. Chim. Acta* **2005**, *548*, 1 – 10.
[10] a) G. Han, D. Kim, Y. Park, J. Bouffard, Y. Kim, *Angew. Chem. Int. Ed.* **2015**, *54*, 3912 – 3916; *Angew. Chem.* **2015**, *127*, 3984 – 3988; b) M. E. Østergaard, P. J. Hrdlicka, *Chem. Soc. Rev.* **2011**, *40*, 5771 – 5788; c) A. A. Martí, S. Jockusch, N. Stevens, J. Ju, N. J. Turro, *Acc. Chem. Res.* **2007**, *40*, 402 – 409; d) Y. Wang, J. Chen, Y. Chen, W. Li, C. Yu, *Anal. Chem.* **2014**, *86*, 4371 – 4378.
[11] a) M. Yoshizawa, J. Nakahawa, K. Kumazawa, M. Nagao, M. Kawano, T. Ozeki, M. Fujita, *Angew. Chem. Int. Ed.* **2005**, *44*, 1810 – 1813; *Angew. Chem.* **2005**, *117*, 1844 – 1847; b) V. Maurizot, M. Yoshizawa, M. Kawano, M. Fujita, *Dalton Trans.* **2006**, 2750 – 2756; c) S. Sato, O. Morohara, D. Fujita, Y. Yamaguchi, K. Kato, M. Fujita, *J. Am. Chem. Soc.* **2010**, *132*, 3670 – 3671.
[12] A. Blatov, *IUCr CompComm Newsletter* **2006**, *7*, 4 (TOPOS is available at http://www.topos.ssu.samara.ru/).
[13] T. H. Noh, E. Heo, K. H. Park, O.-S. Jung, *J. Am. Chem. Soc.* **2011**, *133*, 1236 – 1239.
[14] H. Lee, T. H. Noh, O.-S. Jung, *Angew. Chem. Int. Ed.* **2013**, *52*, 11790 – 11795; *Angew. Chem.* **2013**, *125*, 12006 – 12011.
[15] H. Lee, T. H. Noh, O.-S. Jung, *CrystEngComm* **2013**, *15*, 1832 – 1835.
[16] A. L. Spek, *PLATON: A Multipurpose Crystallographic Tool*, Utrecht University, Utrecht, The Netherlands, **1999**.
[17] a) J. M. Robertson, V. C. Sinclair, J. Trotter, *Acta Crystallogr.* **1961**, *14*, 697 – 704; b) J. Tanaka, *Bull. Chem. Soc. Jpn.* **1963**, *36*, 1237 – 1249.
[18] F. M. Winnik, *Chem. Rev.* **1993**, *93*, 587 – 614.
[19] a) S. Hashimoto, *Chem. Phys. Lett.* **1996**, *252*, 236 – 242; b) F. L. Cozens, M. Régimbald, H. García, J. C. Scaiano, *J. Phys. Chem.* **1996**, *100*, 18165 – 18172; c) X. Liu, J. K. Thomas, *Chem. Mater.* **1994**, *6*, 2303 – 2308; d) X. Liu, K.-K. Iu, J. K. Thomas, *J. Phys. Chem.* **1989**, *93*, 4120 – 4128.
[20] G. Calzaferri, *Langmuir* **2012**, *28*, 6216 – 6231.
[21] E. Fišerová, M. Kubala, *J. Lumin.* **2012**, *132*, 2059 – 2064.
[22] a) S. Siva, J. Thulasidhasan, N. Rajendiran, *Spectrochim. Acta Part A* **2013**, *115*, 559 – 567; b) N. Rajendiran, R. K. Sankaranarayanan, G. Venkatesh, *Bull. Chem. Soc. Jpn.* **2014**, *87*, 797 – 808.
[23] C. P. Brock, J. D. Dunitz, *Acta Crystallogr. Sect. B* **1990**, *46*, 795 – 806.
[24] A. Eisfeld, J. S. Briggs, *Chem. Phys.* **2006**, *324*, 376 – 384.

Received: April 20, 2015
Revised: May 20, 2015
Published online: June 18, 2015

